



Stabilization of Mn(II) and Mn(III) in mononuclear complexes derived from tridentate ligands with N₂O donors: Synthesis, crystal structure, superoxide dismutase activity and DNA interaction studies

Kaushik Ghosh ^{*}, Nidhi Tyagi, Pramod Kumar, Udai P. Singh, Nidhi Goel

Department of Chemistry, Indian Institute of Technology, Roorkee, Roorkee 247 667, Uttarakhand, India

ARTICLE INFO

Article history:

Received 5 May 2009

Received in revised form 17 September 2009

Accepted 21 September 2009

Available online 26 September 2009

Keywords:

Manganese complexes

Crystal structure

Electrochemistry

Superoxide dismutase

DNA binding

Nuclease activity

ABSTRACT

A new family of tridentate ligands PhimpH (2-((2-phenyl-2-(pyridin-2-yl)hydrazono)methyl)phenol), N-PhimpH (2-((2-phenyl-2-(pyridin-2-yl)hydrazono)methyl)naphthalen-1-ol), Me-PhimpH (2-(1-(2-phenyl-2-(pyridin-2-yl)hydrazono)ethyl)phenol) have been synthesized and characterized. The ligands PhimpH and N-PhimpH after deprotonation react with manganese(II) and manganese(III) starting materials affording [Mn(Phimp)₂] (**1**), [Mn(Phimp)₂](ClO₄) (**2**), [Mn(N-Phimp)₂] (**3**), [Mn(N-Phimp)₂](ClO₄) (**4**). Complexes [Mn(Phimp)₂] (**1**) and [Mn(N-Phimp)₂] (**3**) convert to [Mn(Phimp)₂]⁺ (cation of **2**) and [Mn(N-Phimp)₂]⁺ (cation of **4**) respectively upon oxidation. Ligand Me-PhimpH stabilized only manganese(III) centre resulting [Mn(Me-Phimp)₂](ClO₄) (**5**). The molecular structures of [Mn(Phimp)₂], **1** and [Mn(Phimp)₂](ClO₄), **2** were determined by single crystal X-ray diffraction. X-ray crystal structures of **1** and **2** have revealed the presence of distorted octahedral MnN₄O₂ coordination sphere having meridionally spanning ligands. Electrochemical studies for the complexes showed Mn(II)/Mn(III), (*E*_{1/2} = 0.14–0.40 V) and Mn(III)/Mn(IV), (*E*_{1/2} = 0.80–1.06 V) couples vs. Ag/AgCl. The redox properties were exploited to examine superoxide dismutase (SOD) activity using Mn(II)/Mn(III) couple. The complexes **1**, **2**, **4** and **5** have been revealed to catalyze effectively the dismutation of superoxide (O₂⁻) in xanthine–xanthine oxidase–nitro blue tetrazolium assay and IC₅₀ values were found to be 0.29, 0.39, 1.12 and 0.76 μM respectively. DNA interaction studies with complex **2** showed binding of DNA in a non-intercalative pathway. Complexes **1**, **2** and **4** exhibited nuclease activity in presence of H₂O₂ and inhibition of activity was noted in presence of KI.

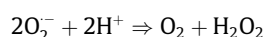
© 2009 Elsevier Inc. All rights reserved.

1. Introduction

Manganese, an essential element for human, is widely distributed in nature and is second in terms of its terrestrial abundance among the first row transition metals [1]. In biosystem several enzymes namely superoxide dismutase (SOD) [2], oxalate oxidase [3], lipoxygenase (LO) [4], catalase [5] etc. require manganese as cofactor for their catalytic activities. In biological reactions manganese sometime acts as a Lewis acid, on the other hand, it could participate in redox reactions by flipping its +2, +3 and +4 oxidation states [6]. Hence it has plural roles in biosystem. However, the role of manganese in oxygen evolving complex (OEC) of photosystem-II (PSII) is unique [2]. Coordination chemistry of manganese has been exploited for the structural and functional modelling of metalloprotein e.g. mimicking of OEC in PSII [7]. Other applications are catalytic activity studies [8] and synthesis of photolabile metal

nitrosyl complexes [9]. Stabilization of manganese oxidation states has been implicated in manganese toxicity [10]. However, our curiosity originated from the great demand of manganese chemistry with ligands having phenolato donors for the mimicking of SOD activity. Moreover, it has been documented in the literature that native SOD as well as small molecule SOD mimics exhibit nuclease activity [11,12]. Hence we were also interested to study DNA interaction as well as nuclease activity studies.

Superoxide dismutases are important class of redox enzymes which are responsible for the disproportionation of superoxide ion (O₂⁻) produced by one electron reduction of oxygen. The redox reaction is shown below:



Superoxide ion is known to be involved in oxidative stress [13] and this reactive species is responsible for several diseases like reperfusion injury, arthritis, neuronal apoptosis, cancer and acquired immunodeficiency syndrome [14]. These metalloenzymes can perform this catalytic redox cycle by several metal ions namely

^{*} Corresponding author. Tel.: +91 1332 285365; fax: +91 1332 2735601.
E-mail address: ghoshfcy@iitr.ernet.in (K. Ghosh).

copper/zinc or manganese or iron [15] or nickel [16]. Manganese complexes, which mimic the activity of superoxide dismutase enzyme, are used for the destruction of detrimental superoxide ions [14,17,18] and in several cases as therapeutic agents [14,17]. Salen complexes of manganese and its derivatives were extensively used for the mimicking of SOD activity [17,19]. However, in very few instances other than salen, ligands with phenolato donor were used [20,21].

Interaction of DNA with transition metal complexes has gained considerable current interest due to its various applications in cancer research and nucleic acid chemistry [22,23]. Although cisplatin and carboplatin are in use, there are several side effects of these chemotherapeutic drugs [24]. Among other transition metal complexes, copper [25] and ruthenium [26,27] complexes are used now-a-days extensively to study metal complex–DNA interactions. However, report of biologically relevant and lesser toxic manganese complexes [17] are fewer [28–35] compared to copper and ruthenium. Only manganese–salen related [28,29] complexes were used for DNA interaction and nuclease activity studies, however, other than salen, to the best of our knowledge Zhang et al. [32] and Bochu and co-workers [34] used ligands affording phenolato donor.

Hence, we designed three tridentate ligands (shown in Scheme 1) containing single phenolato donor along with pyridine and imine donors. Synthesis and spectroscopic characterization of the new family of ligands and their mononuclear manganese complexes are described here. Molecular structures of two representative complexes were determined by X-ray crystallography. Investigation of electrochemical studies prompted us to examine superoxide dismutase activity of these complexes. We have determined IC_{50} values for these complexes using xanthine–xanthine oxidase–nitrobluetetrazolium (NBT) assay. We also report the interaction studies of this family of manganese complexes with DNA and their nuclease activity.

2. Experimental

2.1. Materials

All the solvents used were reagent grade. Removal of all solvents was carried out under reduced pressure. Toluene, diethylether, dimethylsulfoxide (DMSO), dimethylformamide (DMF), chloroform and dichloromethane were purified by distillation over 4 Å molecular sieves and stored over sieves. Methanol was purified by distillation over 3 Å molecular sieves and stored over sieves. Acetonitrile, acetone were dried by refluxing and distillation over P_2O_5 (0.5%, w/v) [36]. Analytical grade reagents salicylaldehyde, *o*-hydroxyacetophenone (SRL, Mumbai, India), 2-hydroxy-1-naphthaldehyde (Sigma Aldrich, Steinheim, Germany), triethylamine (Thomas Baker, India), sodium perchlorate and tert-butylhydroperoxide (t BuOOH) (Himedia Laboratories Pvt. Ltd, Mumbai, India), sodium hydride (Acros organics, USA), $MnCl_2 \cdot 4H_2O$, $Mn(CH_3COO)_2 \cdot 4H_2O$ (Merck Limited, Mumbai, India) $Mn(ClO_4)_2 \cdot 6H_2O$, $Mn(CH_3COO)_3 \cdot 2H_2O$ (Sigma Aldrich, Steinheim, Germany) were used as obtained. $[Mn(DMF)_6](ClO_4)_3$ was prepared according to the method reported in the literature [17].

Xanthine, nitro blue tetrazolium (NBT) and catalase were obtained from Himedia and xantine oxidase (XO) from bovine milk, agarose (molecular biology grade) and ethidium bromide (EB) were purchased from Sigma. The supercoiled pBR322 DNA and calf thymus DNA (CT-DNA) were purchased from Bangalore Genei (India). Tris buffer was prepared in deionised water.

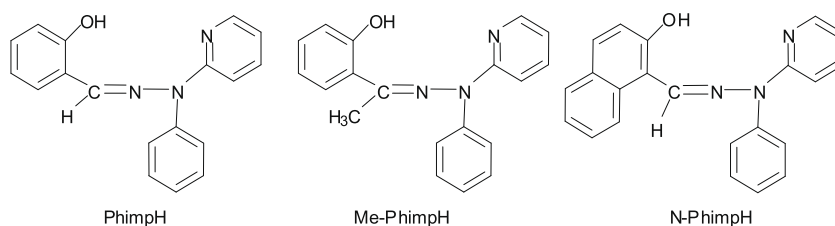
2.2. Methods

2.2.1. Physical measurements

Elemental analyses were carried out microanalytically at Elemental Vario EL III. Melting points were obtained using Perfit (India) melting point apparatus. IR spectra were obtained as KBr pellets with Thermo Nicolet Nexus FT-IR spectrometer, using 50 scans and were reported in cm^{-1} . GC-MS data were obtained on a quadrupole Perkin Elmer Clarus 500 MS coupled to a Perkin Elmer Clarus 500 GC fitted with an Elite-1 column and mass detector was operated at 70 eV. Electronic absorption spectra were recorded in dichloromethane, acetonitrile, DMF or DMSO solvents with an Evolution 600, Thermo Scientific UV–visible spectrophotometer. Emission quenching titrations were carried out on Varian fluorescence spectrophotometer. 1H and ^{13}C NMR were recorded on Bruker AVANCE, 500.13 MHz spectrometer, chemical shift for 1H NMR spectra are related to internal standard Me_4Si for all residual protium in the deuterated solvents. Magnetic susceptibilities were determined at 297 K with Vibrating Sample Magnetometer model 155, using nickel as a standard. Diamagnetic corrections were carried out with Pascal's increments [37]. Molar conductivities were determined in DMF at 10^{-3} M at 25 °C with a Systronics 304 conductometer. Cyclic voltammetry measurements were carried out using a CHI-600C electroanalyzer in dichloromethane and acetonitrile. A conventional three-electrode arrangement consisting of platinum wire as auxiliary electrode, glassy-carbon as working electrode and $Ag(s)/AgCl$ electrode as reference electrode, was used. These measurements were performed in the presence of 0.1 M tetrabutylammonium perchlorate (TBAP) as the supporting electrolyte, using complexes concentration 10^{-3} M in dichloromethane and acetonitrile. The ferrocene/ferrocenium couple was found at $E_{1/2} = +0.42$ (72) V vs. $Ag/AgCl$ under the same experimental conditions. All experiments were performed at room temperature, and solutions were thoroughly degassed with nitrogen prior to beginning the experiments, and during the measurements nitrogen atmosphere was maintained.

2.3. Synthesis of the ligands

2-(1-phenylhydrazinyl)pyridine was prepared according to the method reported [38] in the literature. Ligands PhimpH (2-((2-phenyl-2-(pyridin-2-yl)hydrazono)methyl)phenol), N-PhimpH (2-((2-phenyl-2-(pyridin-2-yl)hydrazono)methyl)naphthalen-1-ol), Me-PhimpH (2-(1-(2-phenyl-2-(pyridine-2-yl)hydrazono)ethyl)phenol) were synthesized by reacting 2-(1-phenylhydrazinyl)pyridine with salicylaldehyde, 2-hydroxy-1-naphthaldehyde and *o*-hydroxyacetophenone respectively in methanol. Details of their synthesis are described in the Supporting Information.



Scheme 1. Schematic drawing of tridentate Schiff's base ligands and abbreviations.

2.4. Synthesis of metal complexes

Perchlorate salts of metal complexes with organic ligands are potentially explosive. Only small quantities of these compounds should be prepared and handled with proper protection. All the complexes were prepared by more than one procedure. One method is described here and the rest are described in the [Supporting Information](#).

2.4.1. Synthesis of [Mn(Phimp)₂](ClO₄)(1)

Complex **1** was synthesized using three different manganese(II) salts separately, however overall procedure was the same. A batch of triethylamine (Et₃N) (133.3 mg, 1.32 mmol) was added to stirred solution of ligand (PhimpH) (381.0 mg, 1.32 mmol) in 10 mL dichloromethane. After stirring for 30 min, a batch of Mn(ClO₄)₂·6H₂O (238.0 mg, 0.66 mmol) in 10 mL methanol was added dropwise. The color of solution changed to orange. After 3 h of stirring, solvent was evaporated to give orange solid which was washed with small amount of methanol, diethylether and dried *in vacuo*. Orange block shaped crystals appeared by diethylether diffusion in dichloromethane/methanol (1:1) solution of the complex within 24 h. Yield: 545.6 mg, (65.6%). IR data (KBr, $\nu_{\max}/\text{cm}^{-1}$): 1598, $\nu_{\text{C=Nimine}}$, 1301, $\nu_{\text{C-Ophenol}}$. UV-visible [CH_2Cl_2 , λ_{\max}/nm ($\epsilon/\text{M}^{-1}\text{cm}^{-1}$): 399 (10,780), 334 (20,520), 310 (20,260), 240 (27,800). μ_{eff} (297 K): 5.87 μ_{B} . $\Lambda_{\text{M}}/\Omega^{-1}\text{cm}^2\text{mol}^{-1}$ (in DMF): 6 (neutral and nonelectrolyte). Anal. Calcd for C₃₆H₂₈N₆O₂Mn: C, 68.46; H, 4.43; N, 13.31. Found: C, 68.40; H, 4.50; N, 13.49.

2.4.2. Synthesis of [Mn(Phimp)₂](ClO₄)(2)

A batch of ligand (PhimpH) (578.0 mg, 2.00 mmol) was dissolved in 7 mL of dichloromethane, methanol and water (2.0:4.5:0.5). After stirring for 10 min, a batch of Mn(CH₃COO)₃·2H₂O (268.0 mg, 1.00 mmol) was added dropwise, the color of solution changed to dark brown. After 15 min stirring sodium perchlorate (140.0 mg, 1.00 mmol) was added to the above reaction mixture. Brown solid precipitated out within 30 min, reaction mixture was further stirred for 3 h. After 3 h of stirring, reaction mixture was filtered; dark brown solid obtained was washed with excess of methanol and dried *in vacuo*. Dark brown block shaped crystals appeared by slow evaporation of a solution of complex **2** in acetonitrile/diethylether (5 mL/3 drop) after a week at room temperature. Yield: 680.0 mg, (46.6%). IR data (KBr, $\nu_{\max}/\text{cm}^{-1}$): 1608, $\nu_{\text{C=Nimine}}$, 1344, $\nu_{\text{C-Ophenol}}$, 1096, 622, $\nu_{\text{ClO}_4^-}$. UV-visible [CH_3CN , λ_{\max}/nm ($\epsilon/\text{M}^{-1}\text{cm}^{-1}$): 421 (4798), 341 (17,791), 306 (18,640), 245 (31,034). μ_{eff} (297 K): 4.69 μ_{B} . $\Lambda_{\text{M}}/\Omega^{-1}\text{cm}^2\text{mol}^{-1}$ (in DMF): 59 (1:1). Anal. Calcd for C₃₇H₃₂N₆O₇ClMn: C, 58.19; H, 4.19; N, 11.01. Found: C, 58.11; H, 4.12; N, 11.51.

2.4.3. Synthesis of [Mn(N-Phimp)₂](3)

A batch of sodium hydride (NaH) (7.7 mg, 0.32 mmol) was added to stirred solution of ligand (N-PhimpH) (101.7 mg, 0.30 mmol) in toluene (15 mL) under the continuous flow of nitrogen atmosphere. After stirring for 30 min, a batch of Mn(ClO₄)₂·6H₂O (54.3 mg, 0.15 mmol) in 5 mL methanol was added dropwise, the color of solution changed from yellow to orange. After 3 h of stirring in nitrogen atmosphere, reaction mixture was concentrated to 5 mL, orange solid separated out which was filtered. This orange solid was washed with excess of toluene and small amount of methanol and dried *in vacuo*. Yield: 128.6 mg, (58.5%). IR data (KBr, $\nu_{\max}/\text{cm}^{-1}$): 1605, $\nu_{\text{C=Nimine}}$, 1325, $\nu_{\text{C-Ophenol}}$. UV-visible [CH_2Cl_2 , λ_{\max}/nm ($\epsilon/\text{M}^{-1}\text{cm}^{-1}$): 448 (24,063), 429 (24,900), 385 (33,479), 332 (38,502), 253 (78,887). μ_{eff} (297 K): 5.49 μ_{B} . $\Lambda_{\text{M}}/\Omega^{-1}\text{cm}^2\text{mol}^{-1}$ (in DMF): 8.2 (neutral and nonelectrolyte). Anal. Calcd for C₄₄H₃₂N₆O₂Mn: C, 72.22; H, 4.37; N, 11.49. Found: C, 72.32; H, 4.39; N, 11.55.

2.4.4. Synthesis of [Mn(N-Phimp)₂](ClO₄)(4)

A batch of triethylamine (Et₃N) (17.2 mg, 0.17 mmol) was added to stirred solution of ligand (N-PhimpH) (57.6 mg, 0.17 mmol) in 10 mL of dichloromethane/methanol (1:1). After stirring for 30 min, a batch of Mn(ClO₄)₂·6H₂O (61.5 mg, 0.17 mmol) in 5 mL methanol was added dropwise, the color of solution changed from yellow to orange and after 2–3 h the color of solution changes to dark brown. After 12 h of stirring 5 mL of diethylether was added to above reaction mixture, brown solid separated out which was filtered washed with small amount of methanol and dried *in vacuo*. Yield: 85.2 mg, (60.2%). IR data (KBr, $\nu_{\max}/\text{cm}^{-1}$): 1611, $\nu_{\text{C=Nimine}}$, 1331, $\nu_{\text{C-Ophenol}}$, 1090, 622, $\nu_{\text{ClO}_4^-}$. UV-visible [CH_3CN , λ_{\max}/nm ($\epsilon/\text{M}^{-1}\text{cm}^{-1}$): 510 (4920), 448 (21,307), 415 (13,460), 384 (35,307), 363 (35,307), 331 (35,384), 317 (33,384), 248 (84,307). μ_{eff} (297 K): 4.97 μ_{B} . $\Lambda_{\text{M}}/\Omega^{-1}\text{cm}^2\text{mol}^{-1}$ (in DMF): 61 (1:1). Anal. Calcd for C₄₄H₃₂N₆O₆ClMn: C, 63.57; H, 3.85; N, 10.11. Found: C, 63.45; H, 3.50; N, 10.08.

2.4.5. Synthesis of [Mn(Me-Phimp)₂](ClO₄)(5)

A batch of sodium hydride (NaH) (24.0 mg, 1.00 mmol) was added to stirred solution of ligand (Me-PhimpH) (303.0 mg, 1.00 mmol) in dichloromethane (5 mL). After stirring for 15 min, a batch of [Mn(DMF)₆](ClO₄)₃ (395.0 mg, 0.50 mmol) in 10 mL acetonitrile was added dropwise; the color of solution changed from yellow to dark brown. After 3 h of stirring 5 mL of diethylether was added to above reaction mixture and a brown solid separated out which was filtered, washed with small amount of methanol and dried *in vacuo*. Yield: 482.3 mg, (63.6%). IR data (KBr, $\nu_{\max}/\text{cm}^{-1}$): 1603, $\nu_{\text{C=Nimine}}$, 1345, $\nu_{\text{C-Ophenol}}$, 1095, 622, $\nu_{\text{ClO}_4^-}$. UV-visible [CH_3CN , λ_{\max}/nm ($\epsilon/\text{M}^{-1}\text{cm}^{-1}$): 421 (7830), 348 (16,980), 233 (52,670), 217 (59,070). μ_{eff} (297 K): 4.77 μ_{B} . $\Lambda_{\text{M}}/\Omega^{-1}\text{cm}^2\text{mol}^{-1}$ (in DMF): 54 (1:1). Anal. Calcd for C₃₈H₃₂N₆O₆ClMn: C, 60.11; H, 4.21; N, 11.07. Found: C, 60.13; H, 4.58; N, 10.88.

2.5. X-ray structure determination

The X-ray data collection and processing for **1** and **2** were performed on Bruker Kappa Apex-II CCD diffractometer by using graphite monochromated Mo-K α radiation ($\lambda = 0.71070 \text{ \AA}$) at 293 K and 296 K respectively. Crystal structures were solved by direct methods. Structure solution, refinement and data output were carried out with the SHELXTL program [39,40]. All non-hydrogen atoms were refined anisotropically. Hydrogen atoms were placed in geometrically calculated positions and refined using a riding model. Images were created with the DIAMOND program [41].

2.6. Measurement of superoxide dismutase activity

Superoxide dismutase activity of complexes **1**, **2**, **4** and **5** were determined by indirect method using nitro blue tetrazolium (NBT) assay. In this method superoxide anion is generated *in situ* enzymatically by xanthine/xanthine oxidase system and detected spectrophotometrically by reduction of NBT which produced a formazan dye of blue color. Absorbance at 560 nm got increased because of production of formazan dye [42]. However, the increase rate of the absorbance was reduced with the increase of complexes concentration. The assay was carried out in phosphate buffer (50 mM) at pH 7.8 using 0.2 mM xanthine, 0.12 mM NBT, 0.07 U/mL xanthine oxidase and catalase 1000 U/mL (final volume = 750 μL). The tested compounds were dissolving in DMSO/DMF (for **1** and **5** in DMSO and **2** and **4** in DMF) and the final concentration of DMSO/DMF in reaction mixture was 0.1% in phosphate buffer at pH 7.8. The reaction was started by adding 0.07 U/mL xanthine oxidase and measurement was started after 15 min for each experiment.

2.7. DNA-binding studies by spectroscopic titration and cleavage experiments

The experiments were carried out in 0.1 M phosphate buffer at pH 7.2 using a solution of calf thymus DNA (CT-DNA) which gave a ratio of absorbance at 260 nm and 280 nm (A_{260}/A_{280}) of ca. 1.8, indicating that the CT-DNA was sufficiently protein free [43]. The concentration of DNA solution was determined by UV-visible absorbance at 260 nm. The extinction coefficient ϵ_{260} was taken as 6600 cm^{-1} as reported in literature [44]. Absorbance titration experiments were carried out with a complex concentration of $23 \mu\text{M}$ varying the CT-DNA concentration from 0 to $68 \mu\text{M}$.

Fluorescence quenching experiments were carried out by the successive addition of 0–7 μM of the manganese complex to the DNA ($25 \mu\text{M}$) solutions containing 5 μM EB in 0.1 M phosphate buffer (pH 7.2) these sample were excited at 510 nm and emission were observed between 530 and 550 nm.

Cleavage of plasmid DNA was monitored by using agarose gel electrophoresis. Supercoiled pBR32 DNA (200 ng) in TBE (pH 8.2) was treated with manganese complexes ($100 \mu\text{M}$) dissolved in DMF (10%) in the presence or absence of additives. The oxidative DNA cleavage by the complexes were studied in the presence of H_2O_2 (200–400 μM , oxidizing agent) and KI (400 μM , radical scavenger). The samples were incubated for 1.5 h at 37°C , added loading buffer (25% bromophenol blue and 30% glycerol). The agarose gel (0.8%) containing 0.4 $\mu\text{g}/\text{mL}$ of EB was prepared and the electrophoresis of the DNA cleavage products was performed on it. The gel was run at 60 V for 2 h in TBE buffer and the bands were identified by placing the stained gel under an illuminated UV lamp. The fragments were photographed by using gel documentation system (BIO RAD).

3. Results and discussion

3.1. Syntheses and characterization of ligands and their metal complexes

The tridentate ligands PhimpH, N-PhimpH and Me-PhimpH were synthesized and their characterizations were established by elemental analysis, UV-visible, IR, GC-MS spectrometry, and NMR (^1H and ^{13}C) spectroscopic studies (shown in Supporting Information). $[\text{Mn}(\text{Phimp})_2]$ (**1**) was synthesized by the reaction of the deprotonated ligand with manganese(II) starting materials. $[\text{Mn}(\text{Phimp})_2](\text{ClO}_4)$ (**2**) was prepared by manganese(III) starting materials as well as *via* the oxidation of **1** by $^t\text{BuOOH}$.

$[\text{Mn}(\text{N-Phimp})_2]$ (**3**) was prepared by manganese(II) starting materials in inert atmosphere. In presence of oxygen, **3** undergoes oxidation to $[\text{Mn}(\text{N-Phimp})_2]^+$. The manganese(III) derivative **4** was independently prepared by the reaction of deprotonated ligand with $[\text{Mn}(\text{DMF})_6](\text{ClO}_4)_3$. In case of Me-PhimpH the deprotonated ligand does not stabilize manganese(II) centre and in all of our synthetic attempts we ended up with $[\text{Mn}(\text{Me-Phimp})_2](\text{ClO}_4)$ (**5**). This may be due to the presence of electron donating methyl ($-\text{Me}$) group attached to the ligand [45]. The synthetic procedures of **1**, **2**, **3**, **4**, **5** and their conversions (*vide infra*) have been summarized in Scheme 2.

The azomethine ($-\text{HC}=\text{N}-$) characteristic band in IR for the free ligand was observed at $\approx 1607\text{--}1620 \text{ cm}^{-1}$. Coordination of the nitrogen to the metal centre reduced the electron density in the azomethine moiety and thus lowered the ($-\text{HC}=\text{N}-$) frequency [46]. Decrease in stretching frequencies for $\nu_{-\text{HC}=\text{N}}$ in $[\text{Mn}(\text{Phimp})_2]$ and $[\text{Mn}(\text{N-Phimp})_2]$ clearly indicates the ligation of azomethine nitrogen ($-\text{HC}=\text{N}-$) to metal centre. The $\nu_{-\text{HC}=\text{N}}$ for $[\text{Mn}(\text{Phimp})_2](\text{ClO}_4)$, $[\text{Mn}(\text{N-Phimp})_2](\text{ClO}_4)$ and $[\text{Mn}(\text{Me-Phimp})_2](\text{ClO}_4)$ are 1608, 1611 and 1603 cm^{-1} respectively. IR bands near 1090 cm^{-1}

together with a band at 623 cm^{-1} were found in all manganese(III) complexes (**2**, **4** and **5**). The lack of splitting of these two bands suggests the presence of non-coordinated perchlorate ion to the metal centre [47]. A high intensity band at ($\approx 1297\text{--}1324 \text{ cm}^{-1}$) in the Schiff bases can be assigned as phenol C–O stretching. Shift of $\nu_{\text{C-O}}$ to higher frequency supports deprotonation and the formation of metal oxygen bond [48]. It is further supported by disappearance of the broad $\nu_{\text{O-H}}$ band in IR spectra of all metal complexes. The molar conductivity measurements in DMF at ca. 10^{-3} M determined at 25°C for complexes **1** and **3** were found to be 6.0 and $8.0 \Omega^{-1} \text{ cm}^2 \text{ mol}^{-1}$ respectively whereas the same for **2**, **4** and **5** were 59.0, 61.0 and $54.0 \Omega^{-1} \text{ cm}^2 \text{ mol}^{-1}$ respectively. These values for **1** and **3** confirm the neutral electrolyte behaviour whereas values for **2**, **4** and **5** clearly indicate uni-univalent (1:1) electrolyte behaviour in solution [49]. For complexes **1** and **3**, room temperature (297 K) magnetic moments were 5.87 and 5.49 μ_{B} respectively, predicting the stabilization of high-spin d^5 manganese(II) in the above two complexes. The magnetic moment values for **2**, **4** and **5** were 4.69, 4.97 and 4.77 μ_{B} respectively, which were expected for a high-spin magnetically dilute d^4 manganese(III) ion, indicating little or no antiferromagnetic interaction [50]. The absorption maxima at 400 nm for complex **1** and 430, 450 nm for complex **3** were assigned to be ligand-to-metal charge transfer (LMCT) transitions [51]. The bands near $\sim 420 \text{ nm}$ respectively for **2**, **4** and **5** were assigned to phenolato oxygen to manganese(III) ligand-to-metal charge transfer (LMCT) transition [52]. However, **4** possesses another two absorption maxima at $\sim 450 \text{ nm}$ ($\epsilon = 21307 \text{ M}^{-1} \text{ cm}^{-1}$) and $\sim 510 \text{ nm}$ ($\epsilon = 4920 \text{ M}^{-1} \text{ cm}^{-1}$) which were also of charge transfer type [53].

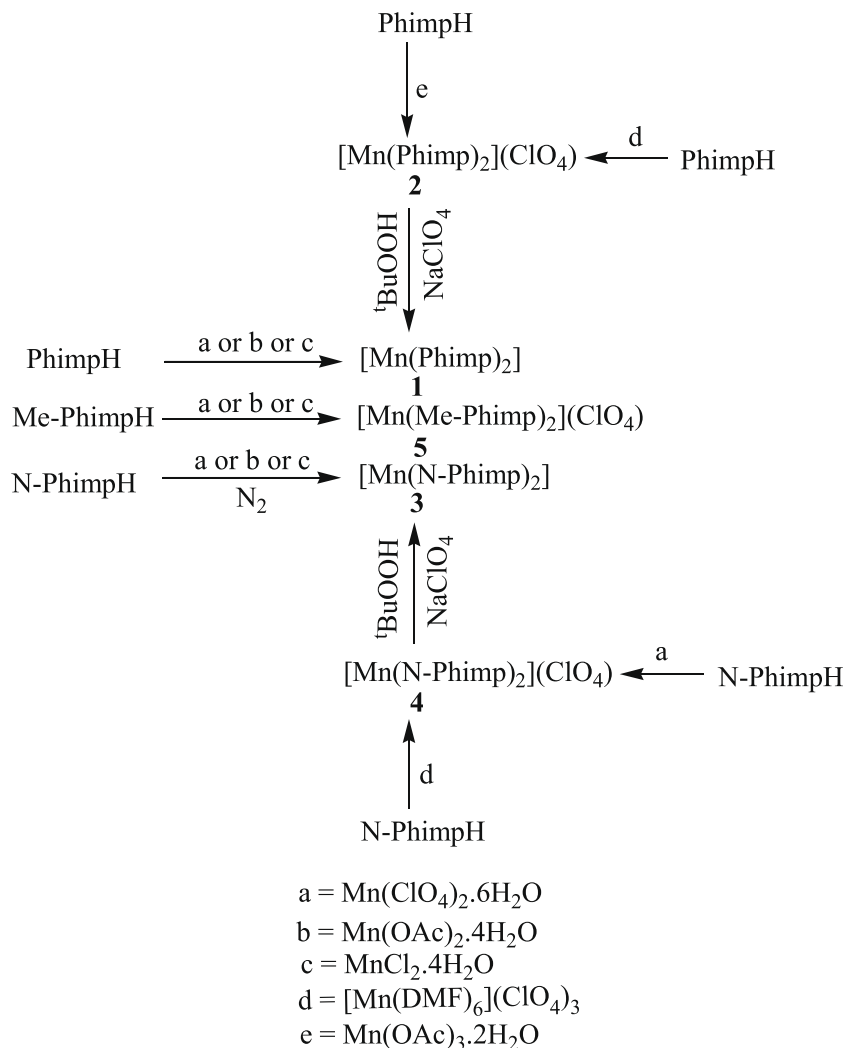
3.2. Interconversions

Characteristic UV-visible spectra of the synthesized manganese complexes in this report prompted us to monitor their interconversion (shown in Scheme 2) through UV-visible spectral studies. Interconversion of **1** to cation of **2** is shown in Fig. 1 whereas that of **3** to cation of **4** is shown in Fig. 2. Disappearance of the peak at 399 nm confirms the formation of $[\text{Mn}^{\text{III}}(\text{Phimp})_2]^+$ as shown in Fig. 1. The decrease in intensity of peaks at 429 nm and 448 nm and increase in intensity of peaks at 384 nm in Fig. 2 indicate the formation of cation of **4** from **3**. The time dependent plots (inset of Fig. 2a and b) clearly show higher rate of conversion of oxidised product in presence of $^t\text{BuOOH}$ as compared to the conversion in presence of oxygen. Hence complexes **2** and **4** could be synthesized by the oxidation of **1** and **3** respectively. Detailed experimental procedure is described in Supporting Information. Characterization of **2** and **4** derived from the oxidation of **1** and **2** by $^t\text{BuOOH}$ gave rise to similar data in IR spectra, conductivity measurement, magnetic moment measurement and electrochemical investigation. We were unable to find the reason for the deviation of the UV-visible data.

3.3. Description of the structures

In order to get the structure of the new family of ligands, single crystals of representative ligand PhimpH were grown by slow evaporation of a dichloromethane solution. Molecular structure of PhimpH was solved by single crystal X-ray diffraction and described in the Supporting Information. The crystal structure gave rise to C=N bond distance of $1.283(3) \text{ \AA}$ which is similar to the reported value of $1.282(3) \text{ \AA}$ [46].

Molecular structures of manganese complexes $[\text{Mn}(\text{Phimp})_2]$ (**1**) and $[\text{Mn}(\text{Phimp})_2](\text{ClO}_4)$ (**2**) are depicted in Figs. 3 and 4 respectively. All the crystallographic parameters are tabulated in Table 1 and selected bond distances and bond angles are listed in Table 2. Crystals of complex **1** were obtained from diethylether diffusion to



Scheme 2.

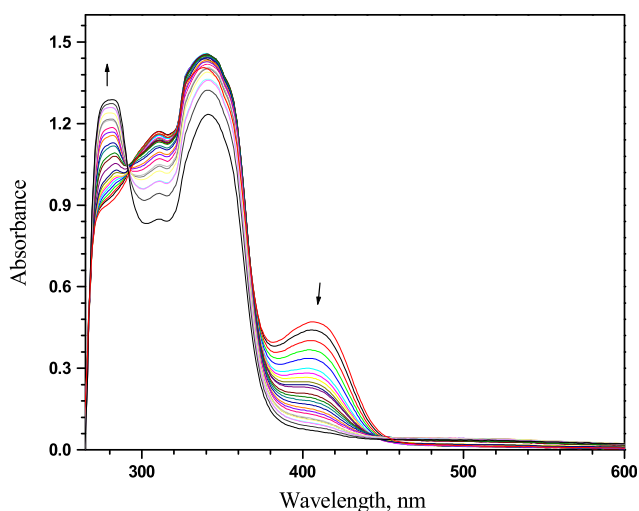


Fig. 1. Titration of $[\text{Mn}(\text{Phimp})_2]$ (**1**) with tBuOOH : spectra were recorded after successive addition of $5 \mu\text{L}$ of $(0.1 \text{ M}) \text{tBuOOH}$ to $10 \mu\text{L}$ of $5.5 \times 10^{-6} \text{ M}$ solution of $[\text{Mn}(\text{Phimp})_2]$ (**1**) in DMF (1 mL) at 25°C .

a solution of **1** in dichloromethane–methanol (1:1) mixture. Compound **1** crystallized in monoclinic space group $C2/c$ consisting of neutral mononuclear manganese(II) complex in N_4O_2 donor set.

In complex **1** the molecule lies on a twofold axis of symmetry and complete structure of the molecule was obtained after growing. The deprotonated ligand PhimpH is coordinated meridionally to the central manganese ion in both complexes **1** and **2**. In both complexes **1** and **2** the metal centre is coordinated by two *trans* imine nitrogens, two *cis* pyridine nitrogen and two *cis* phenolato donors in distorted octahedral fashion. In complex **1**, Mn– N_{py} distance is $2.255(2) \text{ \AA}$ which is consistent with the reported manganese(II) Schiff base complexes [46,54,55]. Similarly Mn– $\text{O}_{\text{phenolato}}$, ($2.0405(18) \text{ \AA}$) bond distance is shorter than that of structurally characterized $[\text{Mn}^{\text{II}}\text{L}](\text{ClO}_4)$, (Mn– $\text{O}_{\text{phenolato}}$ distance, $2.078(5) \text{ \AA}$, where L is heptadentate ligand) and $[\text{Mn}(\text{pyo}_3\text{tren})]^{2+}$ ion (Mn– $\text{O}_{\text{phenolato}}$ distance, $2.192(3) \text{ \AA}$, where pyo₃tren is also a heptadentate ligand) [56,57]. Mn– N_{imine} distance $2.2984(17) \text{ \AA}$ is also closely related with reported data [56,58,59]. The MnN_4O_2 coordination shows a considerable distortion because of ligand's rigidity. Thus the angles at the metal centre [N2–Mn–N2; $153.94(9)^\circ$, O1–Mn–N1; $100.9(3)^\circ$, O1–Mn–N1; $151.24(6)^\circ$ (shown in Table 2)] show large deviation from ideal octahedron.

Complex $[\text{Mn}(\text{Phimp})_2](\text{ClO}_4)$, (**2**) was crystallized after slow evaporation of a solution of **2** in acetonitrile–diethylether. It was crystallized in trigonal space group $P3_121$. The distortion of perfect octahedral geometry was manifested by N2–Mn1–N1 angle of $74.96(12)^\circ$, N1–Mn1–N1; $166.57(16)^\circ$ (shown in Table 2) which differ significantly from ideal 90° and 180° . In complex **2**, Mn– N_{py}

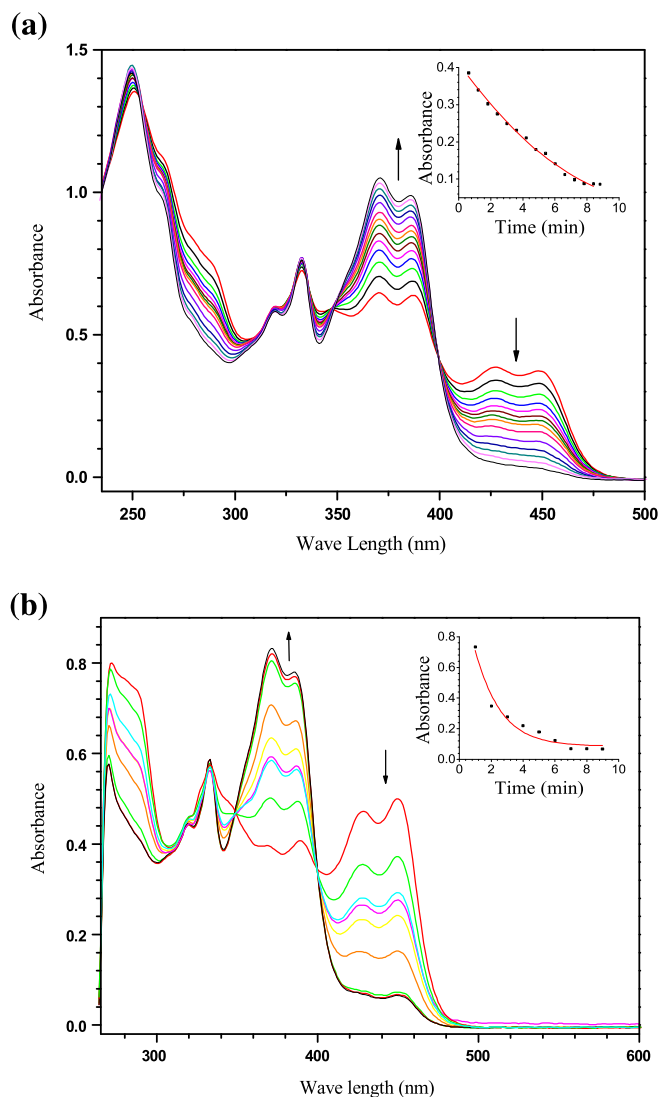


Fig. 2. (a) Aerial oxidation for conversion of **3** to cation of **4** by repetitive scan of $10 \mu\text{L}$ of 2.87×10^{-3} mM of $[\text{Mn}(\text{N-Phimp})_2]$ in dichloromethane (1 mL) and changes in spectral patterns were recorded after each 0.6 min interval. (b) Titration of $[\text{Mn}(\text{N-Phimp})_2]$ by $5 \mu\text{L}$ of 3.25×10^{-3} mM with $0.2 \mu\text{L}$ of $t\text{BuOOH}$ (0.01 M) and the changes in spectral patterns were recorded after 1 min interval in DMF (1 mL) at 25°C .

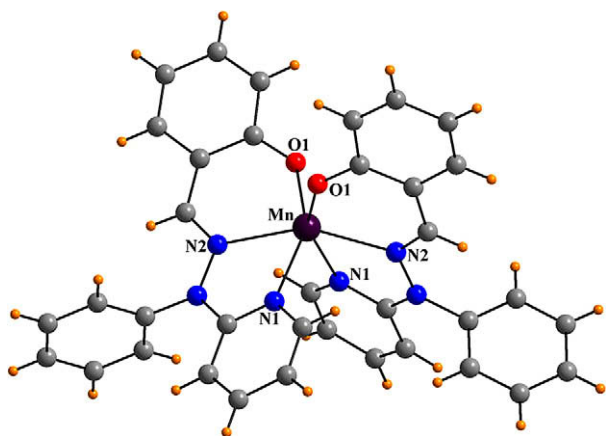


Fig. 3. Ball-and-stick representation of the crystal structure of $[\text{Mn}(\text{Phimp})_2]$ (**1**), atoms are shown as sphere of arbitrary diameter, and the molecule lies on a twofold axis of symmetry.

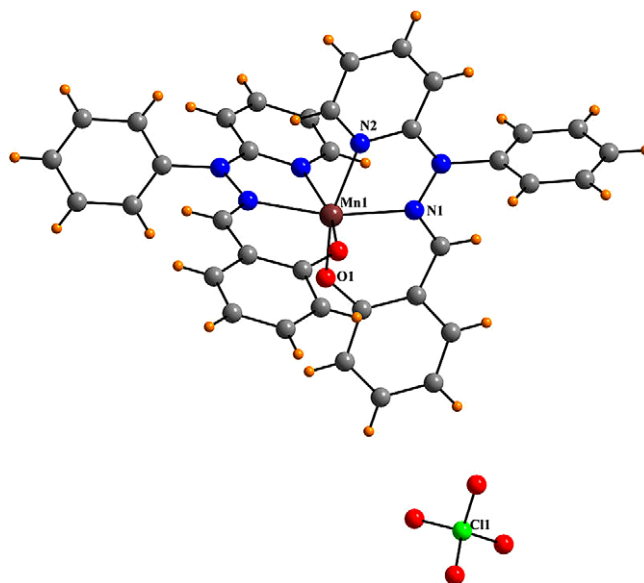


Fig. 4. Ball-and-stick representation of the crystal structure of $[\text{Mn}(\text{Phimp})_2](\text{ClO}_4)$ (**2**), atoms are shown as sphere of arbitrary diameter.

and $\text{Mn}-\text{O}_{\text{phenolato}}$ distances are consistent with the reported data [21,60,61]. $\text{Mn}-\text{N}_{\text{imine}}$ bond distances were found to be $2.176(3) \text{ \AA}$ which is longer than the usual reported values of $2.001(6) \text{ \AA}$ in $[\text{Mn}^{\text{III}}(\text{L})\text{Cl}]^+$ where L is Schiff base ligand [58] and other structurally characterized manganese(III) complexes [21,48,61,62]. A d^4 system of manganese(III) is susceptible to undergo Jahn–Teller distortion and is expected to show elongation of *trans* bonds. In our complex the *trans* imine bond lengths are longer than the usual distances, may be due to Jahn–Teller distortion [51].

Examination of packing diagram of complexes **1** and **2** revealed non-covalent interactions. These types of non-covalent and hydrogen bonding interactions are very important in the crystal engineering and supramolecular frameworks [63]. The data for non-covalent interaction are described in Table S3 and Fig. S23 in Supporting Information.

There is no conjugation between the pyridine ring and the phenolato ring; however they remain in the same plane in the ligand as well as in metal complexes. The angle between the phenyl ring attached to the nitrogen and plane containing phenolato ring and pyridine ring is 88.14° in ligand, 86.38° in complex **1** and 87.84° in complex **2** (phenyl ring vs. *mer* plane). Comparing the structure of free ligand and the ligand bound to the metal centre, the following facts were observed. A very little change in $\text{N1}-\text{C8}-\text{N2}$ and $\text{O1}-\text{C1}-\text{C6}$ angles of the ligand was observed in the complexes **1** and **2**. On the other hand due to the coordination of imine nitrogen to the metal centre in both complexes, $\text{N3}-\text{C7}-\text{C6}$ angle of the ligand was decreased by $\sim 7^\circ$. The $\text{Mn}-\text{N}_{\text{py}}$, $\text{Mn}-\text{O}_{\text{phenolato}}$ and $\text{Mn}-\text{N}_{\text{imine}}$ bond lengths in case of **2** are lower than that of **1** which confirms stabilization of manganese(II) centre for **1** and manganese(III) centre for **2**. This is consistent with our magnetic moment data.

3.4. Redox properties and SOD activity

In order to examine the influence of the newly synthesized ligands on metal centre, we investigated the electrochemical properties of the five (**1–5**) complexes isolated and characterized in this report. The representative voltammograms of complexes **1** and **5** are shown in Fig. 5 (figures for **2**, **3** and **4** are shown in Supporting Information (Fig. S21)), and the redox potentials for all the

Table 1
Crystallographic data for complexes [Mn(Phimp)₂] (**1**) and [Mn(Phimp)₂](ClO₄) (**2**).

Empirical formula	C ₃₆ H ₂₈ MnN ₆ O ₂ (1)	C ₃₆ H ₂₈ ClMnN ₆ O ₆ (2)
Color	Orange	Brown
Formula weight (g mol ⁻¹)	631.58	731.03
Temperature (K)	293(2)	296(2)
λ (Å) (Mo-Kα)	0.71073	0.71073
Crystal system	Monoclinic	Trigonal
Space group	C2/c	P3 ₁ 21
a (Å)	18.599(5)	10.775(2)
b (Å)	9.786(5)	10.775(2)
c (Å)	17.368(5)	26.197(5)
α (°)	90.00	90.00
β (°)	96.407(5)	90.00
γ (°)	90.00	120.00
V (Å ³)	3141(2)	2633.9(10)
Crystal size (mm)	0.24 × 0.19 × 0.13	0.27 × 0.23 × 0.17
Z	4	3
ρ _{calcd} (g cm ⁻³)	1.336	1.383
F(0 0 0)	1308	1600
θ range for data collection	2.20–28.27	2.18–28.19
Index ranges	–24 < h < 24, –12 < k < 13, –22 < l < 23	–14 < h < 14, –14 < k < 14, –30 < l < 34
Refinement method	Full matrix least-squares on F ²	Full matrix least-squares on F ²
Data/restraints/parameters	3835/0/204	4331/0/227
GOF ^a on F ²	1.017	1.775
R1 ^b (I > 2σ(I))	0.0405	0.0613
R1 (all data)	0.0812	0.0696
wR2 ^c (I > 2σ(I))	0.1193	0.2054
wR2 (all data)	0.1577	0.2163

^a GOF = $[\sum[w(F_o^2 - F_c^2)^2]/M - N]^{1/2}$ (M = number of reflections, N = number of parameters refined).

^b R1 = $\sum||F_o| - |F_c||/\sum F_o$.

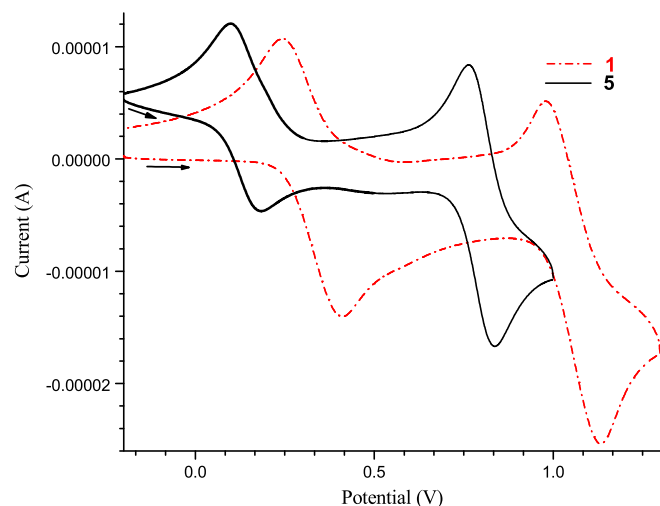
^c wR2 = $[\sum[w(F_o^2 - F_c^2)^2]/\sum[w(F_o^2)^2]]^{1/2}$.

Table 2

Selected bond distances (Å) and bond angles (°) at the manganese centre for [Mn(Phimp)₂] (**1**) and [Mn(Phimp)₂](ClO₄) (**2**). In complex **1** the molecule lies on a twofold axis of symmetry. In complexes **1** and **2** the complete molecular structure were available after growing.

[Mn(Phimp) ₂] (1)	[Mn(Phimp) ₂](ClO ₄) (2)	
Bond distances (Å)		
Mn–O1	2.0405(18)	Mn1–O1 1.879(3)
Mn–N1	2.255(2)	Mn1–N2 2.099(3)
Mn–N2	2.2985(17)	Mn1–N1 2.176(3)
Bond angles (°)		
O1–Mn–O1	98.08(13)	O1–Mn1–O1 95.8(3)
O1–Mn–N2	81.31(6)	O1–Mn1–N1 87.23(11)
O1–Mn–N1	116.53(6)	O1–Mn1–N1 101.84(13)
N2–Mn–N2	153.94(9)	N1–Mn1–N1 166.57(16)
N1–Mn–N2	91.45(7)	N2–Mn1–N1 74.96(12)
N1–Mn–N1	70.08(6)	N2–Mn1–N1 85.74(18)
O1–Mn–N1	91.21(11)	N2–Mn1–N2 95.05(12)
O1–Mn–N1	92.33(8)	O1–Mn1–N2 91.89(15)
O1–Mn–N1	151.24(6)	O1–Mn1–N2 161.72(12)

complexes are described in Table 3. The neutral uncomplexed ligands do not show any cyclic voltammogram over the range from –1.0 to 1.4 V; hence all the curves were attributed to the redox activity of our complexes. The shapes of the cyclic voltammograms for all the complexes are similar with two redox peaks. For complex **1** both the peaks are quasi-reversible whereas complex **2** showed reversible peaks. For complexes **3** and **4** both the redox peaks are approximately reversible, however, both redox couples are reversible in **5**. From the data (Table 3), it has been shown that one electron is involved in this redox process. The wave detected at 0.14–0.40 V vs. Ag/AgCl has been considered as one-electron-redox

**Fig. 5.** Cyclic voltammograms of a 10⁻³ M solution of **1** in dichloromethane and **5** in acetonitrile, in presence of 0.1 M tetrabutylammonium perchlorate (TBAP), using working electrode: glassy-carbon, reference electrode: Ag/AgCl; auxiliary electrode: platinum wire, scan rate 0.1 V/s.**Table 3**

Electrochemical data for the redox couples Mn(II)/Mn(III) and Mn(III)/Mn(IV) at 298 K^a vs. Ag/AgCl.

Complex	Mn(II)/Mn(III)			Mn(III)/Mn(IV)		
	E _{pa} (V)	E _{pc} (V)	E _{1/2} ^b (ΔE _p ^c)(V)	E _{pa} (V)	E _{pc} (V)	E _{1/2} ^b (ΔE _p ^c)(V)
1	0.410	0.243	0.327 (167)	1.133	0.979	1.056 (154)
2	0.323	0.247	0.285 (76)	1.014	0.930	0.927 (84)
3	0.388	0.293	0.341 (95)	1.020	0.916	0.968 (104)
4	0.454	0.366	0.410 (88)	0.949	0.843	0.896 (106)
5	0.184	0.101	0.143 (83)	0.838	0.766	0.802 (72)

^a Measured in dichloromethane for **1**, **3** and in acetonitrile for **2**, **4** and **5** with 0.1 M tetrabutylammonium perchlorate (TBAP).

^b Data from cyclic voltammetric measurements; E_{1/2} is calculated as average of anodic (E_{pa}) and cathodic (E_{pc}) peak potentials E_{1/2} = 1/2(E_{pa} + E_{pc}).

^c ΔE_p = E_{pa} – E_{pc} at scan rate 0.1 V/s.

process attributed to the oxidation of [Mn^{II}L₂] to [Mn^{III}L₂]⁺ (where L = Phimp⁻, N–Phimp⁻, Me–Phimp⁻) indicating Mn(II)/Mn(III) redox couple. However, another redox wave detected at E_{1/2} = 0.80–1.06 V vs. Ag/AgCl is described as Mn(III)/Mn(IV) redox couple. These data match with the values reported [20,58,64] for the manganese complexes with similar ligand frame. E_{1/2} values for Mn(II)/Mn(III) and Mn(III)/Mn(IV) couples in **5** are 0.143 V and 0.802 V respectively. These data for **5** are comparatively smaller than that other complexes (Table 3) which is probably due to electron donating (–Me) group attached to the ligand [45].

Superoxide dismutation is a redox process and hence electrochemical properties of manganese complexes are very important for SOD activity studies. Several reports [20,60,65–71] are there by which one can select a manganese complex that could mimic SOD activity considering the electrochemical properties. Our electrochemical data showed the Mn(II)/Mn(III) couple, responsible for the catalytic activity, was within the proper range [60,69]. These prompted us to investigate the SOD activity of the complexes. IC₅₀ value for SOD activity has been defined as the concentration of a particular tested compound for 50% inhibition of NBT reduction by superoxide produced in the xanthine/xanthine oxidase system. The IC₅₀ data of the SOD activity assay are described in Table 4 and inhibition curve for complex **1** is shown in Fig. 6 (curves for complexes **2**, **4** and **5** are shown in Supporting Information (Fig. S22)). According to our data complex **2** shows the lowest

Table 4
IC₅₀ values and kinetic catalytic constant of **1**, **2**, **4** and **5** complexes.

Complex	IC ₅₀ ^a (μM)	k _{MCCF} (M ⁻¹ s ⁻¹) ^b × 10 ⁷
1	0.29	4.09
2	0.39	3.04
4	1.12	1.06
5	0.76	1.56

^a IC₅₀ values are the average of two replicate experiments. ^b k_{MCCF} were calculated by $K = k_{\text{NBT}} \times [\text{NBT}] / \text{IC}_{50}$, k_{NBT} (pH 7.8) = $5.94 \times 10^4 \text{ M}^{-1} \text{ s}^{-1}$ [73,74].

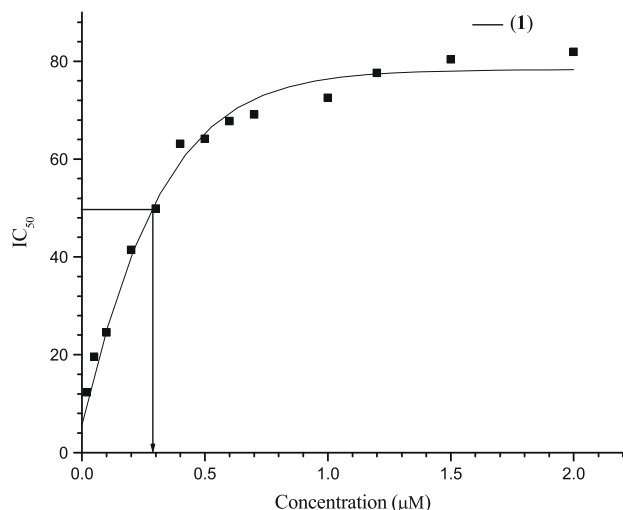


Fig. 6. SOD activity of complex **1** (in DMF) in the xanthine oxidase–nitro blue tetrazolium (NBT) assay.

IC₅₀ value, on the other hand complex **4** shows the highest IC₅₀ value. Comparing the IC₅₀ data for all Mn(III) complexes, **2** showed the lowest and **4** showed the highest IC₅₀ value. Complexes **1** and **2** utilized the same Mn(II)/Mn(III) redox couple to destroy superoxide ions however, complex **1** (for its +2 oxidation state) converted O₂⁻ to O₂²⁻ whereas other Mn(III) complexes converted O₂⁻ to O₂ using same redox couple. Due to the instability of **3** in air we were unable to examine its activity. The IC₅₀ value of complex **5** is consistent with the data reported by Kitajima et al. [68], Xiang et al. [69] and Cisnetti et al. [20]. Complex **4** gave rise to IC₅₀ value of 1.12 μM which is better than the data reported by Faulkner et al. [70], Lin et al. [60], Deroche et al. [71], Ouyang et al. [67] and Policar et al. [65]. However the IC₅₀ values (0.29 μM and 0.39 μM respectively) for complexes **1** and **2** are not only the best among the new family of manganese complexes we report here but also among the very good SOD mimics known in the literature [66,72].

3.5. DNA-binding studies

To examine the nuclease activity of this family of complexes we extended our investigation by starting DNA interaction with these small molecule SOD mimics [12]. Among all the complexes, **2** was selected for DNA interaction studies due to its solubility in biological buffer solution. Other complexes were not soluble in the condition set for the DNA-binding studies. In order to understand the DNA binding properties of **2**, we followed two techniques namely UV–visible spectral studies and EB fluorescence quenching studies. The experimental results are shown in Figs. 7 and 8 respectively. The intensity of the peak at 307 nm in UV–visible spectra got decreased due to the addition of CT-DNA. A considerable hypochromicity of 4.41% without change in wavelength implies that some interaction occurred between complex **2** and the surface of DNA molecule and the interaction is not an intercalation [75,76].

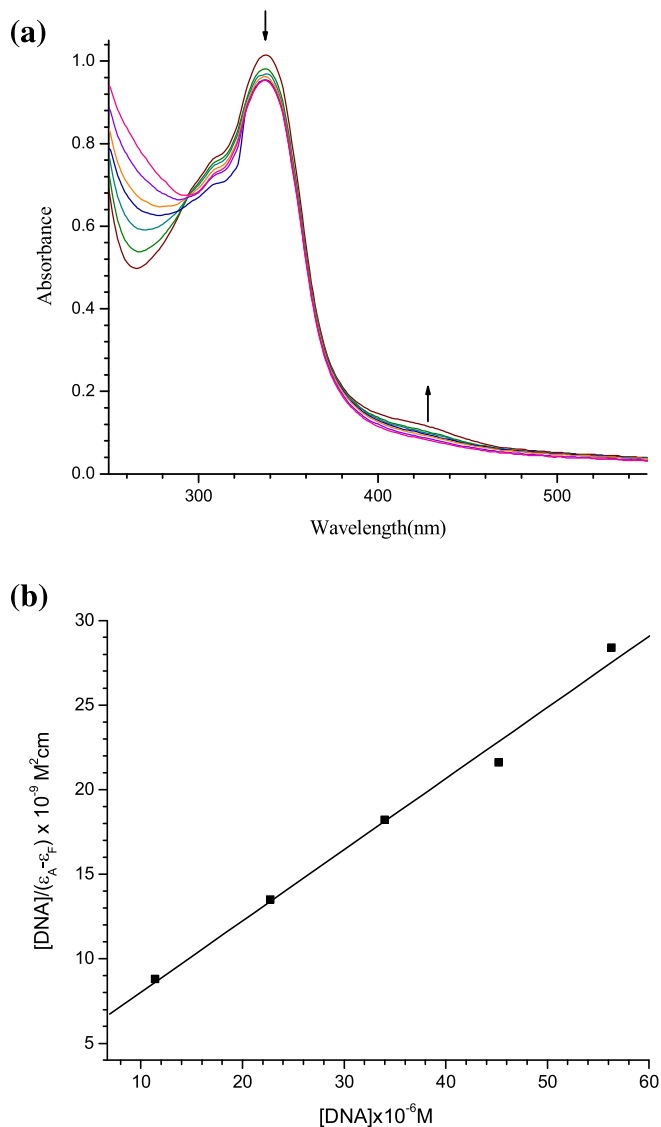


Fig. 7. (a) Absorption spectra of [Mn(Phimp)₂](ClO₄)₂ in 0.1 mM phosphate buffer (pH 7.2) in presence of increasing amounts of DNA ([DNA] = 0–68 μM). (b) Plot of [DNA]/(ε_A - ε_F) vs. [DNA].

The binding strength of complex **2** with CT-DNA could be expressed in terms of intrinsic binding constant K_b , which represents the binding constant per DNA base pair. This constant could be obtained by monitoring the changes in the absorbance at a λ_{max} with increase in concentration of CT-DNA by following the equation [30].

$$[\text{DNA}] / (\varepsilon_A - \varepsilon_F) = [\text{DNA}] / (\varepsilon_B - \varepsilon_F) + 1 / K_b (\varepsilon_B - \varepsilon_F m)$$

where [DNA] is the concentration of DNA in base pairs and ε_A , ε_F and ε_B correspond to the ratio of $A_{\text{abs}} / [\text{complex}]$, the molar absorptivity for the free manganese complex, and the molar absorptivity for the manganese complex in the fully bound form respectively. In the plot of [DNA]/(ε_A - ε_F) vs. [DNA], K_b is given by the ratio of the slope to the Y-intercept. The binding constant K_b was found to be $7.87 \times 10^4 \text{ M}^{-1}$ which is lower than the values reported for the intercalation of manganese complexes [31,77]. The examinations of fluorescence spectral studies were carried out to further exclude the possibility of intercalative binding mode. EB is an intercalator that gives a significant increase in fluorescence emission when bound to DNA, and its displacement from DNA results in a decrease in fluorescence intensity. Addition of **2** to EB-DNA system shows

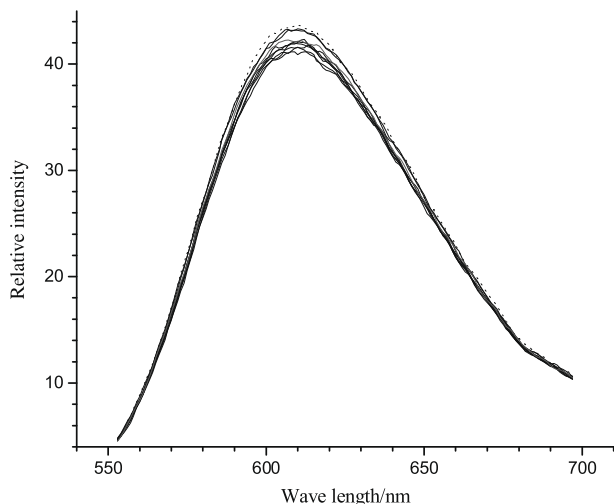


Fig. 8. Fluorescence emission spectra of the EB-CT-DNA ([DNA] = 25 μM) system in absence (dashed line) and presence (solid line) of the complex **2** (0–7 μM).

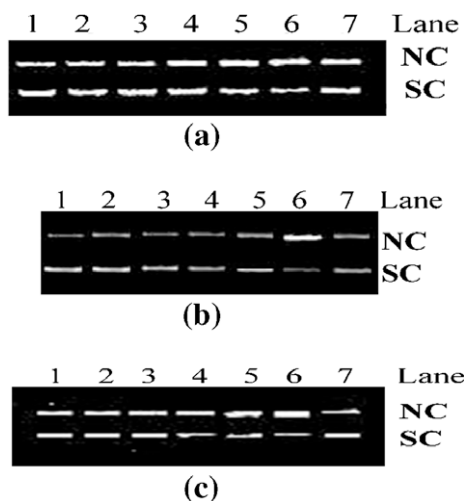


Fig. 9. Gel electrophoresis separations showing the oxidative cleavage of supercoiled pBR322 DNA (200 ng) by complexes (100 μM) **1** (A), **2** (B) and **4** (C) respectively. Complexes **1**, **2** and **4** in 10% DMF incubated at 37 $^{\circ}\text{C}$ for 1.5 h. (A) DNA (Lane 1); DNA + H_2O_2 (150 μM) (Lane 2); DNA + **1** (Lane 3); DNA + **1** + H_2O_2 (150 μM) (Lane 4); DNA + **1** + H_2O_2 (300 μM) (Lane 5); DNA + **1** + H_2O_2 (400 μM) (Lane 6); DNA + **1** + H_2O_2 (150 μM) + KI (300 μM) (Lane 7). (B) DNA (Lane 1); DNA + DMF (2 μL) (Lane 2); DNA + H_2O_2 (150 μM) (Lane 3); DNA + **2** (Lane 4); DNA + **2** + H_2O_2 (150 μM) (Lane 5); DNA + **2** + H_2O_2 (400 μM) (Lane 6); DNA + **2** + H_2O_2 (150 μM) + KI (300 μM) (Lane 7). (C) DNA (Lane 1); DNA + H_2O_2 (150 μM) (Lane 2); DNA + **4** (Lane 3); DNA + **4** + H_2O_2 (150 μM) (Lane 4); DNA + **4** + H_2O_2 (300 μM) (Lane 5); DNA + **4** + H_2O_2 (400 μM) (Lane 6); DNA + **4** + H_2O_2 (150 μM) + KI (300 μM) (Lane 7).

very little change in fluorescence (shown in Fig. 8). The lower K_b value and small change in fluorescence spectral studies indicate the non-intercalative binding interaction with DNA and probable groove binding or external binding is suggested [75,76]. Structure solution for **2** also revealed that the phenyl ring attached to the nitrogen is roughly perpendicular (87.84°) to the ligand binding plane having phenolato ring and pyridine ring. This phenyl ring probably inhibits the intercalation with DNA.

3.6. Nuclease activity

The absorption and fluorescence quenching studies with complex **2** indicated non-intercalative interaction of the manganese

complex with CT-DNA. We further extended our DNA interaction studies by examining the nuclease activity of the complexes. The cleavage of supercoiled pBR322 DNA by the complexes were studied by gel electrophoresis in tris buffer. We performed the nuclease activity in 10% DMF for complexes **1**, **2** and **4**. The strand scissions of plasmid pBR322 were assayed in the presence of H_2O_2 . Examining the data obtained from DNA gel electrophoresis, it is clear that in presence of H_2O_2 the complexes can cleave plasmid pBR322 DNA to a mixture of supercoiled and nicked DNA (shown in Fig. 9). In search of the mechanism of nuclease activity of this family of complexes we investigated the activity in presence of NaN_3 and KI which are known to be singlet oxygen and hydroxyl radical scavengers respectively [76]. No change in nuclease activity in presence of NaN_3 and inhibition of activity in presence of KI were observed. These data indicate that possible role of reactive oxygen species (ROS) is involved in nuclease activity.

4. Conclusions

In this study we prepared tridentate PhimpH, N-PhimpH and Me-PhimpH ligands and characterized the ligands with UV-visible, IR, GC-MS and NMR studies. These ligands after deprotonation were reacted with Mn(II) and Mn(III) starting materials and in all synthetic attempts we ended up with *bis* complexes. Both the Mn(II) and Mn(III) centre were stabilized by the ligand PhimpH and N-PhimpH whereas only Mn(III) complex was isolated and characterized for ligand Me-PhimpH. UV-visible and IR spectral studies, magnetic moment data and conductivity measurements confirm the formation of $[\text{Mn}(\text{Phimp})_2]$ (**1**), $[\text{Mn}(\text{Phimp})_2](\text{ClO}_4)$ (**2**), $[\text{Mn}(\text{N-Phimp})_2]$ (**3**), $[\text{Mn}(\text{N-Phimp})_2](\text{ClO}_4)$ (**4**), $[\text{Mn}(\text{Me-Phimp})_2](\text{ClO}_4)$ (**5**). X-ray crystal structures of complexes **1** and **2** revealed the formation of manganese(II) and manganese(III) complexes respectively and for both complexes ligand was bound to the metal centre in meridional fashion. Bond distances support the stabilization of high-spin manganese(II) in complex **1** and manganese(III) in complex **2**. Investigation of electrochemical studies showed Mn(II)/Mn(III) and Mn(III)/Mn(IV) couples. Our complexes satisfy the properties required for a small molecule SOD mimic. Among them, complexes **1** and **2** with IC_{50} values 0.29 and 0.39 μM respectively provide a novel example of low molecular weight SOD mimics on the basis of activity relationship. DNA-binding studies of complex **2** indicated a non-intercalative interaction and a probable groove binding or external binding with CT-DNA has been suggested. The phenyl ring, which is approximately perpendicular to the ligand binding plane, probably inhibits the intercalation with DNA. Another major finding was that complexes **1**, **2** and **4** exhibited nuclease activity. Hence our small molecule SOD mimics set another example to support the data reported in the literature [12]. Inhibition of the nuclease activity in presence of KI indicated the probable participation of reactive oxygen species in DNA cleavage.

Acknowledgements

KG is thankful to DST, New Delhi, India for SERC FAST Track project support. NT and PK are thankful to CSIR, India for financial assistance. We are thankful to IITR for Faculty Initiation Grant and instrumentation facilities. UPS is thankful to Head, Instrumentation Centre, IIT Roorkee for single crystal X-ray facility.

Appendix A. Supplementary material

Supplementary data associated with this article can be found, in the online version, at [doi:10.1016/j.jinorgbio.2009.09.014](https://doi.org/10.1016/j.jinorgbio.2009.09.014).

References

- [1] D.W. Christianson, *Prog. Biophys. Molec. Biol.* 67 (1997) 217–252.
- [2] J.J.R. Frausto da Silva, R.J.P. Williams, *The Biological Chemistry of the Elements*, Clarendon Press, Oxford, 1993, p. 4.
- [3] E.-J. Woo, J.M. Dunwell, P.W. Goodenough, A.C. Marvier, R.W. Pickersgill, *Nat. Struct. Biol.* 7 (2000) 1036–1040.
- [4] C. Su, E.H. Olliv, *J. Biol. Chem.* 273 (1998) 13072–13079.
- [5] T.L. Stemmler, B.E. Sturgeon, D.W. Randall, R.D. Britt, J.E. Penner-Hahn, *J. Am. Chem. Soc.* 119 (1997) 9215–9225.
- [6] V.L. Pecoraro (Ed.), *Manganese Redox Enzymes*, VCH, New York, 1992.
- [7] S. Mukhopadhyay, S.K. Mandal, S. Bhaduri, W.H. Armstrong, *Chem. Rev.* 104 (2004) 3981–4026.
- [8] G. Yin, A.M. Danby, D. Kitko, J.D. Carter, W.M. Scheper, D.H. Busch, *Inorg. Chem.* 46 (2007) 2173–2180 (and references therein).
- [9] K. Ghosh, A.A. Eroy-Reveles, B. Avila, T.R. Holman, M.M. Olmstead, P.K. Mascharak, *Inorg. Chem.* 43 (2004) 2988–2997.
- [10] L. Quintanar, *Inorg. Chim. Acta* 361 (2008) 875–884.
- [11] W. Jiang, Y. Han, Q. Pan, T. Shen, C. Liu, *J. Inorg. Biochem.* 101 (2007) 667–677.
- [12] M. Devereux, D.O. Shea, A. Kelleth, M. McCann, M. Walsh, D. Egan, C. Deegan, K. Kedziora, G. Rosair, H. Muller-Bunz, *J. Inorg. Biochem.* 101 (2007) 881–892.
- [13] D. Salvemini, C. Muscoli, D.P. Riley, S. Cuzzocrea, *Pulm. Pharmacol. Therapeut.* 15 (2002) 439–447.
- [14] D. Salvemini, Z.-Q. Wang, J.L. Zweier, A. Samouilov, H. Macarthur, T.P. Misko, M.G. Currie, S. Cuzzocrea, J.A. Sikorski, D.P. Riley, *Science* 286 (1999) 304–306.
- [15] I. Bertini, S.J. Gray, S.J. Lippard, J.S. Valentine, *Bioinorganic Chemistry*, University Science Book, Mill Valley, California, 1994.
- [16] D.P. Barondeau, C.J. Kassmann, C.K. Bruns, J.A. Tainer, E.D. Getzoff, *Biochemistry* 43 (2004) 8038–8047.
- [17] D.P. Reley, *Chem. Rev.* 99 (1999) 2573–2588.
- [18] I. Batinić-Haberle, I. Spasojević, R.D. Stevens, P. Hambricht, P. Neta, A. Okamoto-Matsumoto, I. Fridovich, *Dalton Trans.* (2004) 1696–1702.
- [19] F. Fucassi, J.E. Lowe, K.D. Pavey, S. Shah, R.G.A. Faragher, M.H.L. Green, F. Paul, D.O. Hare, P.J. Cragg, *J. Inorg. Biochem.* 101 (2007) 225–232.
- [20] F. Cisnetti, G. Pelosi, C. Policar, *Inorg. Chim. Acta* 360 (2007) 557–562.
- [21] S. Durot, C. Policar, F. Cisnetti, F. Lambert, J.-P. Renault, G. Pelosi, G. Blain, H. Korri-Youssoufi, J.-P. Mahy, *Eur. J. Inorg. Chem.* (2005) 3513–3523.
- [22] N. Farrell, *Coord. Chem. Rev.* 232 (2002) 1–4.
- [23] H. Ali, J.E.V. Lier, *Chem. Rev.* 99 (1999) 2379–2450.
- [24] E. Wong, C.M. Giandomenico, *Chem. Rev.* 99 (1999) 2451–2466.
- [25] S. Mahadevan, M. Palaniandavar, *Inorg. Chem.* 37 (1998) 693–700.
- [26] M.J. Clarke, *Coord. Chem. Rev.* 232 (2002) 69–93.
- [27] Y.K. Yan, M. Melchart, A. Habtemariam, P.J. Sadler, *Chem. Commun.* (2005) 4764–4776.
- [28] D.J. Gravert, J.H. Griffin, *Inorg. Chem.* 35 (1996) 4837–4847 (and references therein).
- [29] S.S. Mandal, N.V. Kumar, U. Varshney, S. Bhattacharya, *J. Inorg. Biochem.* 63 (1996) 265–272.
- [30] A. Dimitrakopoulou, C. Dendrinou-Samara, A.A. Pantazaki, M. Alexiou, E. Nordlander, D.P. Kessissoglou, *J. Inorg. Biochem.* 102 (2008) 618–628 (and references therein).
- [31] Z.-D. Xu, H. Liu, M. Wang, S.-L. Xiao, M. Yang, X.-H. Bu, *J. Inorg. Biochem.* 92 (2002) 149–155.
- [32] S.-S. Zhang, S.-Y. Niu, B. Qu, G.-F. Jie, H. Xu, C.-F. Ding, *J. Inorg. Biochem.* 99 (2005) 2340–2347.
- [33] S. Niu, M. Zhao, R. Ren, S. Zhang, *J. Inorg. Biochem.* 103 (2009) 43–49.
- [34] T. Jun, W. Bochu, Z. Liancai, *Colloids Surf. B* 55 (2007) 149–152.
- [35] S.C.M. Gandini, V.E. Yushmanov, J.R. Perussi, M. Tabak, I.E. Borissevitch, *J. Inorg. Biochem.* 73 (1999) 35–40.
- [36] W.L.F. Armaergo, C.L.L. Chai, *Purification of Laboratory Chemicals*, fifth ed., Butter Heinemann, Elsevier Science, USA, 2002, pp. 85–86.
- [37] R.L. Dutta, A. Syamal, *Elements of Magnetochemistry*, second ed., Affiliated East-West Press, New Delhi, 1993, p. 8.
- [38] A. Kotschy, J. Faragó, A. Csámpai, D.M. Smith, *Tetrahedron* 60 (2004) 3421–3425.
- [39] G.M. Sheldrick, *Acta Cryst. A* 46 (1990) 467–473.
- [40] G.M. Sheldrick, *SHELXTL-NT 2000 Version 6.12*, Reference Manual. University of Gottingen, Pergamon, New York, 1980.
- [41] B. Klaus, University of Bonn, Germany DIAMOND, Version 1.2c, 1999.
- [42] C. Beauchamp, I. Fridovich, *Anal. Biochem.* 44 (1971) 276–287 (and references therein).
- [43] J. Marmur, *J. Mol. Biol.* 3 (1961) 208–218.
- [44] M.E. Reichmann, S.A. Rice, C.A. Thomas, P. Doty, *J. Am. Chem. Soc.* 76 (1954) 3047–3053.
- [45] M. Maneiro, M.R. Bermejo, M.I. Fernández, E. Gómez-Fórneas, A.M. González-Noya, A.M. Tyryshkin, *New J. Chem.* 27 (2003) 727–733.
- [46] O. Pouralimardan, A.-C. Chamayou, C. Janiak, H. Hosseini-Monfared, *Inorg. Chim. Acta* 360 (2007) 1599–1608.
- [47] M.R. Rosenthal, *J. Chem. Educ.* 50 (1973) 331–335.
- [48] M. Maneiro, M.R. Bermejo, A. Sousa, M. Fondo, A.M. González, A. Sousa-Pedrares, C.A. McAuliffe, *Polyhedron* 19 (2000) 47–54.
- [49] W.J. Geary, *Coord. Chem. Rev.* 7 (1971) 81–122.
- [50] O.L. Hoyos, M.R. Bermejo, M. Fondo, A. García-Deibe, A.M. González, M. Maneiro, R. Pedrido, *J. Chem. Soc. Dalton Trans.* (2000) 3122–3127.
- [51] S. Biswas, K. Mitra, S.K. Chattopadhyay, B. Adhikary, *Transition Met. Chem.* 30 (2005) 393–398.
- [52] J.A. Bonadies, M.J. Maroney, V.L. Pecoraro, *Inorg. Chem.* 28 (1989) 2044–2051.
- [53] A. Neves, S.M.D. Erthal, I. Vencato, A.S. Ceccato, Y.P. Mascarenhas, O.R. Nascimento, M. Horner, A.A. Batista, *Inorg. Chem.* 31 (1992) 4749–4755.
- [54] M.E.D. Vries, R.M.L. Crois, G. Roelfes, H. Kooijman, A.L. Spek, R. Hage, B.L. Feringa, *Chem. Commun.* (1997) 1549–1550.
- [55] J. Limburg, J.S. Vrettos, R.H. Crabtree, G.W. Brudivg, J.C.D. Paula, A. Hassan, A.-L. Barra, C. Duboc-Toia, M.-N. Collomb, *Inorg. Chem.* 40 (2001) 1698–1703.
- [56] O. Horner, J.-J. Girerd, C. Philouze, L. Tchertanov, *Inorg. Chim. Acta* 290 (1999) 139–144.
- [57] S. Gou, X. You, K. Yu, J. Lu, *Inorg. Chem.* 32 (1993) 1883–1887.
- [58] L. Sabater, C. Hureau, R. Guillot, A. Aukauloo, *Inorg. Chem.* 45 (2006) 2373–2375.
- [59] S. Naskar, D. Mishra, S.K. Chattopadhyay, M. Corbella, A.J. Blake, *Dalton Trans.* (2005) 2428–2435.
- [60] J. Lin, C. Tu, H. Lin, P. Jiang, J. Ding, Z. Guo, *Inorg. Chem. Commun.* 6 (2003) 262–265.
- [61] J.-P. Costes, F. Dahan, B. Donnadieu, M.-J.R. Douton, M.-I.F. Garcia, A. Bousseksou, J.-P. Tuchagues, *Inorg. Chem.* 43 (2004) 2736–2744.
- [62] A. Panja, N. Shaikh, S. Gupta, R.J. Butcher, P. Banerjee, *Eur. J. Inorg. Chem.* (2003) 1540–1547.
- [63] G.R. Dasiraju, T. Steiner, *The weak hydrogen bond*, in: J. John (Ed.), *Structural Chemistry and Biology*, Oxford University Press, New York, 1999.
- [64] M.U. Triller, D. Pursche, W.-Y. Hsieh, V.L. Pecoraro, A. Rompel, B. Krebs, *Inorg. Chem.* 42 (2003) 6274–6283.
- [65] C. Policar, S. Durot, F. Lambert, M. Cesario, F. Ramiandrasoa, I. Morgenstern-Badarau, *Eur. J. Inorg. Chem.* (2001) 1807–1818.
- [66] R. Kachadourian, I. Batinić-Haberle, I. Fridovich, *Inorg. Chem.* 38 (1999) 391–396.
- [67] X.-M. Ouyang, B.-L. Fei, T.-A. Okamura, W.-Y. Sun, W.-X. Tang, N. Ueyama, *Chem. Lett.* 3 (2002) 362–363.
- [68] N. Kitajima, M. Osawa, N. Tamura, Y. Moro-oka, T. Hirano, M. Hirobe, T. Nagano, *Inorg. Chem.* 32 (1993) 1879–1880.
- [69] D.F. Xiang, C.Y. Duan, X.S. Tan, Q.W. Hang, W.X. Tang, *J. Chem. Soc. Dalton Trans.* (1998) 1201–1204.
- [70] K.M. Faulkner, R.D. Stevens, I. Fridovich, *Arch. Biochem. Biophys.* 310 (1994) 341–346.
- [71] A. Deroche, I. Morgenstern-Badarau, M. Cesario, J. Guilhem, B. Keita, L. Nadjio, C. Houe-Levin, *J. Am. Chem. Soc.* 118 (1996) 4567–4573.
- [72] I. Batinić-Haberle, I. Spasojević, P. Hambricht, L. Benov, A.L. Crumbliss, I. Fridovich, *Inorg. Chem.* 38 (1999) 4011–4022.
- [73] R.F. Pasternack, B. Halliwell, *J. Am. Chem. Soc.* 101 (1979) 1026–1031.
- [74] Z.-R. Liao, X.-F. Zheng, B.-S. Luo, L.-R. Shen, D.-F. Li, H.-L. Liu, W. Zhao, *Polyhedron* 20 (2001) 2813–2821.
- [75] S. Sarkar, A. Mondal, D. Chopra, J. Ribas, K.K. Rajak, *Eur. J. Inorg. Chem.* (2006) 3510–3516.
- [76] J. Chen, X. Wang, Y. Shao, J. Zhu, Y. Zhu, Y. Li, Q. Xu, Z. Guo, *Inorg. Chem.* 46 (2007) 3306–3312.
- [77] Z.-D. Xu, H. Liu, S.-L. Xiao, M. Yang, X.-H. Bu, *J. Inorg. Biochem.* 90 (2002) 79–84.